Microfluidic-Spinning-Directed Microreactors Toward Generation of Multiple Nanocrystals Loaded Anisotropic Fluorescent Microfibers

Yan Zhang, Cai-Feng Wang, Li Chen, Su Chen, and Anthony J. Ryan**

Anisotropic fluorescent hybrid microfibers with distinct optical properties and delicate architectures have aroused special interest because of their potential applications in tissue engineering, drug delivery, sensors, and functional textiles. Microfluidic systems have provided an ideal microreactor platform to produce anisotropic fibers due to their simplified manipulation, high efficiency, flexible controllability, and environmental-friendly chemical process. Here a novel microfiber reactor based on a microfluidic spinning technique for in situ fabrication of nanocrystals loaded anisotropic fluorescent hybrid microfibers is demonstrated. Multiple nanocrystal reactions are carried out in coaxial flow-based microdevices with different geometric features, and various nanocrystals loaded microfibers with solid, string-of-beads and Janus topographies are obtained. Moreover, the resulted anisotropic fluorescent hybrid microfibers present multiple optical signals. This strategy contributes a facile and environmental-friendly route to anisotropic fluorescent hybrid microfibers and might open a promising avenue to multiplex optical sensing materials.

1. Introduction

Similar to the way that touch spots of biological neural networks can generate biological information, anisotropic micro- and nanoscale fibers can be combined to form larger network with multidimensional ordered hierarchical architecture, evoking new collective functions. To this end, much efforts engineer functional microscale fibers to tissue engineering,[1] drug delivery,[2] sensors,[3] and functional textiles.[4] To date, a wide range of methods including self-assembly,[5] electrospinning method,[6,7] electro-hydrodynamic cojetting,[8] and microfluidic approach[9] have been proposed for anisotropic fibers on the micro- and nanoscale. Especially, microfluidic approach brings various advantages such as mild reaction conditions, high selectivity, simplified manipulation, and environmental benign synthesis enabling fabrication of anisotropic microfibers.[10] Over the last decade, a variety of anisotropic microfibers with varied chemical compositions, complex shapes, and diverse functionalities have been developed by using microfluidic spinning based on different solidification methods, processing platforms, or materials.[11–14] However, the exploration of anisotropic hybrid microfibers with more distinct fluorescent information continues to be a hot topic since the reported approaches on artificial network fibers still cannot compare with those of biological tissue network. Although some efforts have already been reported on fabrication of fluorescent hybrid microfibers by fluorescent dye molecules[4,9] and nanocrystals (NCs),[15,16] in situ formation of fluorescent microarrays during microfluidic spinning process might be still challenging.

In this work, we demonstrated a strategy to facilely construct versatile fiber microreactors via a microfluidic spinning technique (MST). The proposed approach not only provides an ideal microreactor platform with in situ production of high-performance fluorescent nanocrystals in the process of microfiber formation, but also produces hybrid multiple anisotropic microfibers, along with the precise control of reaction temperature, efficient heat and mass transfer, economical use of reactants, and green synthesis route.[17,18] To our knowledge, there have been numerous reports of NCs synthesized in microfluidic reactors based on single-phase continuous flow, segmented or slug flow and droplet flow.[19–22] However, utilizing MST based on coaxial continuous flow to 1D microfiber microreactors for the in situ fabrication of NCs is still rare, especially for the preparation of multiple NCs loaded anisotropic fluorescent microfibers. Herein, we designed coaxial continuous flow-based microdevices with different geometric features, and then programmed multiple NC reactions in the process of microfiber formation. As shown in **Scheme 1**a, a single NC reaction (A+B→C) was done in a half-T-shaped microdevice with two microchannels, along with solid and string-of-beads microfibers. Similarly, dual-NC reactions ($A+B_1 \rightarrow C_1$, $A+B_2 \rightarrow C_2$) were simultaneously carried out in a Y-shaped microdevice with three microchannels, and heterogeneous hydrogel microfibers with

Y. Zhang, Prof. C.-F. Wang, Prof. L. Chen, Prof. S. Chen
State Key Laboratory of Materials-Oriented Chemical Engineering
College of Chemistry and Chemical Engineering
Nanjing Tech University
Nanjing 210009, P.R. China
E-mail: chensu@njtech.edu.cn
Prof. A. J. Ryan
Department of Chemistry
University of Sheffield
Sheffield S3 7HF, UK
E-mail: tony.ryan@sheffield.ac.uk

DOI: 10.1002/adfm.201503680

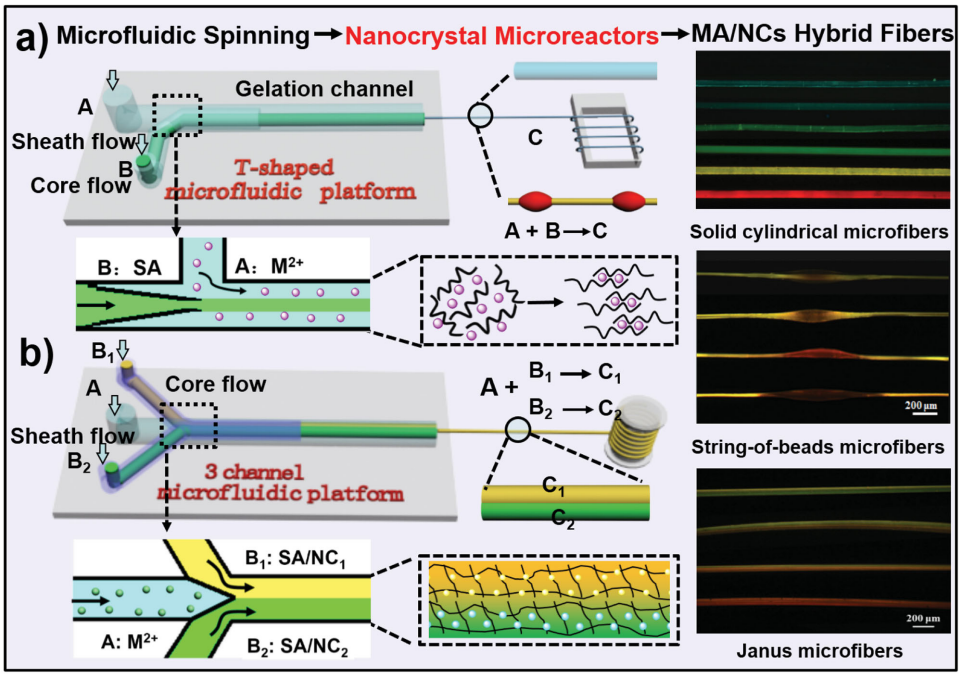

Scheme 1. Schematic illustrations of the coaxial microfluidic spinning devices used for continuously generating nanocrystal loaded alginate fluorescent hybrid microfibers. a) Single nanocrystal reaction (A + B → C) in half-T-shaped microdevice containing two microchannels for fabricating solid cylindrical and string-of-beads microfibers. b) Dual-nanocrystal reactions ($A + B_1 \rightarrow C_1$, $A + B_2 \rightarrow C_2$) in Y-shaped microdevice with three microchannels for fabricating Janus microfibers.

Janus topography were obtained (Scheme 1b). By this design, various fluorescent NCs coded anisotropic fluorescent microfibers were produced in microfiber reactors under a mild and green route. This MST directed microfiber reactors may offer new broad types of microreactors and fundamental insight into chemistry in microfiber reactors. Moreover, both the prepared string-of-beads and Janus anisotropic hybrid microfibers present two different kinds of optical signals. An application of these fibers for multiplexed optical analysis was demonstrated by taking advantage of the virtues of NCs immobilized in the anisotropic microfibers. This strategy may constitute a promising simple way to fabricate a new kind of nanocrystal sensing materials.

2. Results and Discussion

2.1. Synthesis of M-Alginate Fibers by Microfluidic Spinning

We chose here alginate as the hydrogel material for microfiber fabrication because of its rapid gelation in the presence of multivalent metal ions. A microfiber spinning equipment consisting of a syringe pump, a coaxial continuous flow microdevice, and a fiber receiver has been employed for the generation of M-alginate (MA) hydrogel microfibers (**Figure 1**a and Figure S1, Supporting Information).[23,24] Typically, for the fabrication of Ca-alginate fibers in half-T-shaped microfluidic device, the core flow of the sodium alginate (SA) solution (B) was pumped into the microdevice through a needle microchannel, while the Ca^{2+} sheath flow (A) was injected into the region between the inner needle microchannel and the outer silicone rubber hose (Scheme 1a and Figure 1a). At the interface between the two flows, SA was instantly cross-linked due to the diffusion of Ca^{2+} ions into the alginate network. The solidified Ca-alginate fibers were then extruded through an outlet channel and collected continuously (see Video S1, Supporting Information). These decreases in the intensities of C—O (1025 cm^{-1}) and the C—H (2926 cm^{-1}) stretching peak of Ca-alginate, as shown in the FT-IR and IR images (Figure 1c), further confirm the ionic crosslinking between the Ca^{2+} and SA.[25,26] We also fabricated NCs loaded fluorescent hybrid microfibers by incorporating different-sized CdTe NCs into the SA core flow (Figure 1b). At optimal conditions, the spinning procedure exhibited good stability with flow rates of core flow and sheath flow fixed at 40 mL h^{-1} and 25 mL h^{-1}, respectively, and the obtained cylindrical hydrogel microfibers showed an average diameter of 70 μm (Figure 1d).[27] The presented microfluidic spinning process is very rapid and simple for the subsequent generation of hydrogel microfibers, which provides tremendous possibilities for the preparation of anisotropic fluorescent hybrid microfibers with enhanced functionality.

2.2. Production of Single-Metal Nanocrystals in String-of-Beads Microfiber Reactors

After the stable formation of the M-alginate hydrogel microfibers, we explored the possibility of the microfluidic spinning system for in situ fabricating NCs loaded fluorescent hybrid microfibers. It is known that microfluidic approach takes obvious advantages over conventional batch synthesis methods for producing high quality nanocrystals by reason of a reduction

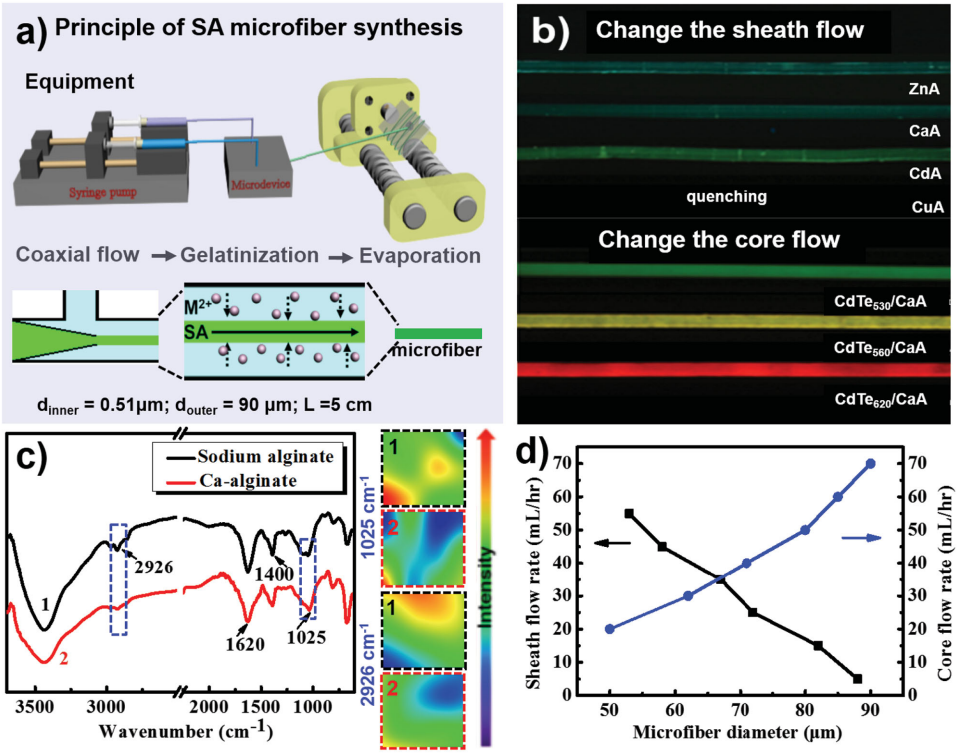

Figure 1. a) Schematic illustrations of the microfluidic spinning equipment with a syringe pump, microdevice, and a fiber receiver and the principle of cross-linking process for generating M-alginate hydrogel microfibers by chemical reactions. b) Fluorescent microscope images of pure M-alginate microfibers and CdTe NCs (λ_{em} = 530, 560, and 620 nm) loaded Ca-alginate microfibers. c) FT-IR spectra and IR images of pure sodium alginate molecule and Ca-alginate hydrogel. d) Relationship between the diameter of microfibers and the core flow rate with a fixed sheath flow rate at 25 mL h^{-1}, and the sheath flow rate with a fixed core flow rate at 40 mL h^{-1}.

in reaction volume and better uniformity in the chemical and thermal environment. Illuminatingly, we extended the microfluidic spinning system to a continuous flow reactor platform to construct a novel microfiber reactor. In addition, by designing coaxial continuous flow microdevices with different geometric features, we made attempts to program multiple NC reactions in the microfiber reactor for achieving diverse NCs coded anisotropic fluorescent microfibers.

Figure 2 shows an example of a single NC reaction (A+B→C) carried out via microfiber reactor in a half-T-shaped microdevice. The core flow (1 wt% SA solution mixed with sulfide source (0.045 M $Na_2S \cdot 9H_2O$)) (B) and sheath flow (0.2 M $CdCl_2 \cdot 2.5H_2O$) (A) were introduced into corresponding inlet, respectively. At the position where the two fluids merged, the sheath flow shaped the focused core flow to form a stable coaxial flow, and then induced diffusion and reaction of Cd^{2+} and S^{2-} (Figure 2a). Due to the coordination and protection of carboxyl group of alginate, it is favorable to passivate the surface defects of nanoparticles, and then making it possible to form fluorescent CdS NCs (C) in CdA microfibers matrix (Figure 2e,f).[28] Unlike the traditional NC synthetic methods relying on high temperature and effective ligands, the proposed microfiber reactors allow NC chemical reactions to be carried out at ambient temperature. More importantly, the NCs were produced and immobilized in the microfiber matrix, hence this is an environmental-friendly synthetic route without heavy metal waste solutions.

Surprisingly, we found that the incorporation of sulfide source resulted in the formation of fluorescent hybrid microfibers with string-of-beads topography, comprising a highly ordered beads and string microstructures, which is entirely different to that obtained from the pure Cd-alginate microfibers. We assume that this might be caused by the following reasons. In the presence of sulfide source, there is a competition between the carboxyl group of SA and S^{2-} for the incoming Cd^{2+} ions. Consequently, a reduction in the rate of chelation between Cd^{2+} ions and alginate carboxyls and concentration differences take place, leading to a pressure pulse in this system. Then the process brings about the release of beads continuously along the fiber for balancing the internal pressure and surface forces.[29] To gain insight into the reaction process, the flow rates of sheath and core fluids were investigated, as these played a vital role in determining the morphology of the microfibers. Faster core flow rates enabled the generation of microfibers with larger beads distance. As depicted in Figure 2c and Figure S2, Supporting Information, the distance shows an increase of about 3 mm as the core flow rate increased from 30 to 70 mL h^{-1} (see Videos S2 and S3, Supporting Information). The sheath flow rate critically affected the bead diameter. By increasing the sheath flow rate from 15 to 55 mL h^{-1}, the bead diameter of hydrated CdA/CdS fiber increases gradually from 0.3 to 2 mm (Figure 2d and Figure S3, Supporting Information). So we can obtain successfully string-of-beads microfibers with controllable bead distance and bead size by controlling the experimental conditions.

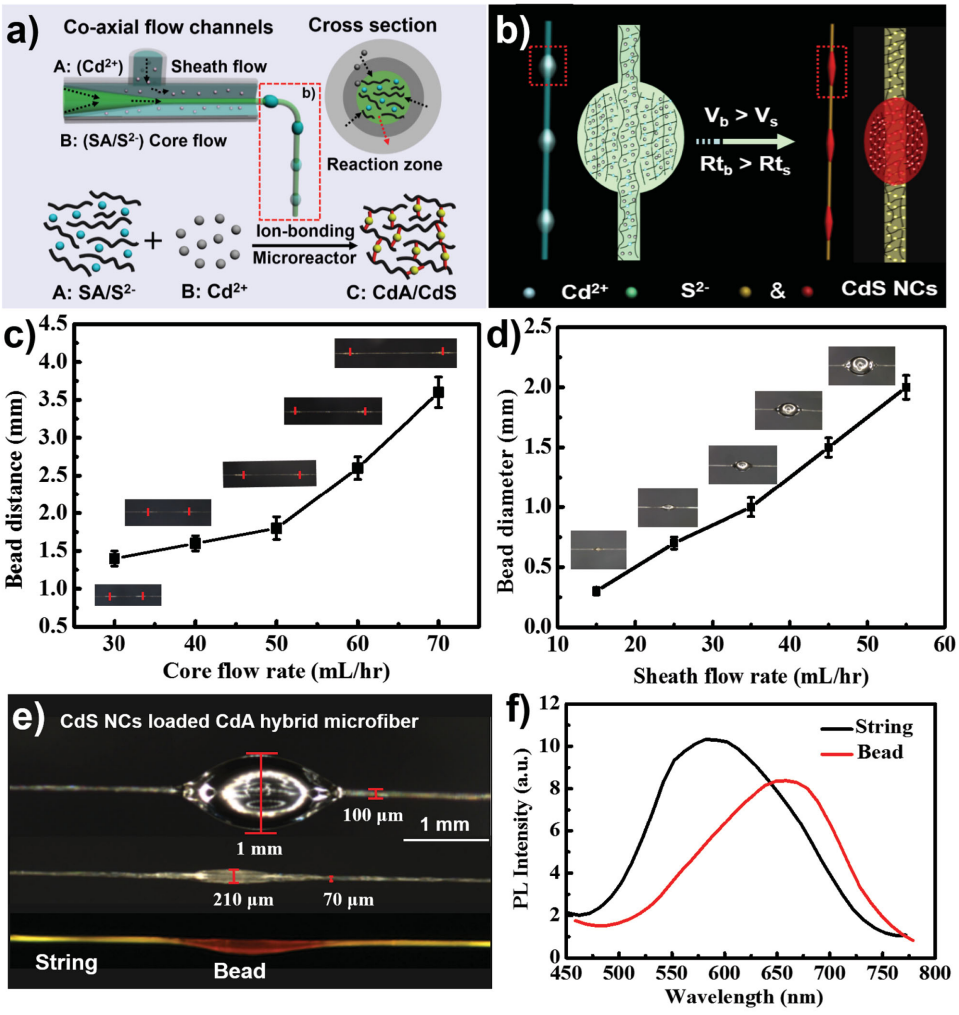

Figure 2. a,b) Schematic illustrations of the formation of the string-of-beads CdA/CdS hybrid microfibers. c) Distance of the beads in dehydrated CdA/CdS fiber as functions of the core flow rate. d) Diameter of the beads in hydrated CdA/CdS fiber as functions of the sheath flow rate. e) Bright-field images of microfibers in hydrated and dehydrated states, and fluorescent microscope image of CdS NCs loaded CdA hybrid microfiber with flow rates fixed at 40 (core flow) and 35 mL h^{-1} (sheath flow). f) The corresponding PL emission spectra of the beads and string of CdA/CdS hybrid microfibers, respectively.

Based on the special string-of-beads geometry, we further explored the optical properties of CdS NCs loaded CdA fluorescent microfibers. Interestingly, the fluorescent photograph under 365 nm UV light reveals that the beads and string along CdA/CdS hybrid microfibers display red and yellow fluorescence (Figure 2e), respectively, with the corresponding maximum PL emission band centered at 650 and 580 nm (Figure 2f). As the ratio of bead diameter to string thickness of the obtained hydrated microfibers is about 10:1 (Figure 2e), we have found that the density of CdS NCs in the beads is higher than those of the strings, and the reaction time (Rt) for the formation of CdS NCs in the beads is longer than those in the strings, so that larger-size NCs are obtained in the beads (Figure 2b). In following work, we further investigated the optical properties of the string-of-beads microfibers with different bead size. As we believed, the bead diameter significantly affects the emission peak positions and PL intensities of the beads of CdA/CdS fluorescent microfibers with only minor effects on the string (Figure S4 and Figure S5, Supporting Information). To our knowledge, the fabrication of such anisotropic fluorescent hybrid microfiber has never been reported. It is predicted that the process of these string-of-beads hybrid microfibers presenting two different signals may be a unique way to produce new fluorescent materials for optical application.

To assess the stability of CdS NCs in the CdA hydrogel matrix, a time-correlated single-photon counting (TCSPC) methodology was further adopted to generate time-resolved photoluminescence. The average fluorescence lifetime of the bead CdS NCs is 3.55 ns, while of string CdS NCs has a common 4.07 ns lifetime (**Figure 3**a and Table S1, Supporting Information), which further confirms that SA polymer could effectively prevent the aggregation of NCs and decrease the defects of NCs. By virtue of chemical incorporation between NCs and hydrogel matrixes, the in situ generated CdS NCs are highly stable without fluorescence quenching over several months (Figure S7, Supporting Information). To further verify

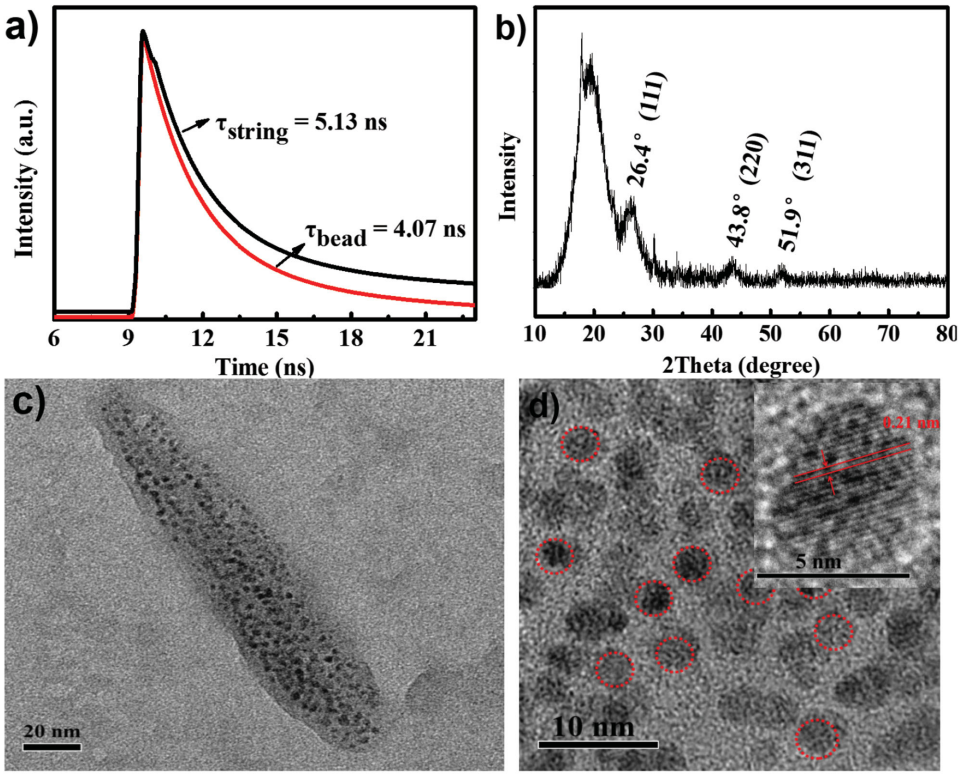

Figure 3. a) Time-resolved fluorescence decay curves of the beads and strings of CdA/CdS hybrid microfibers. b) The XRD pattern of CdA/CdS hybrid fluorescent powder. c) TEM images of CdS NCs in CdA microfibers. d) The HRTEM image of a single nanocrystal.

the existence and distribution of CdS NCs in the CdA hydrogel microfibers, transmission electron microscope (TEM) was employed. As depicted in the typical TEM image of CdS NCs (Figure 3c), the as-prepared NCs appear as the spherical particles showing an excellent dispersion without obvious aggregation. The high-resolution TEM (HRTEM) image (Figure 3d) clearly shows well-resolved lattice fringes for an individual CdS NC, indicating an excellent crystalline structure, meaning the NCs are well preserved in the SA/NCs hybrid microfibers. The fringe spacing is 0.21 nm, corresponding to the (220) plane of cubic CdS. In addition, the crystalline structure of the as-prepared CdA/CdS microfibers was characterized by powder X-ray diffraction (XRD). The diffraction peaks (seen in Figure 3b) of CdA/CdS at 2θ values of 26.4°, 30.6°, 43.8°, 51.9° match with the cubic CdS (JCPDS no.89-0440) and can be indexed to the (111), (200), (220), and (311) planes. The calculated size of CdS NCs in the microfibers is approximately 4 nm from the major diffraction peak (111) (2θ = 26.4°) by the Scherrer equation.[30] The above results clearly demonstrate the successful synthesis of well-defined CdS NCs in CdA hydrogel microfibers.

We also observed the effect of S/Cd molar ratios on the optical properties of CdA/CdS fluorescent hybrid microfibers. As presented in **Figure 4**a, both the positions of peaks of beads and strings have a red shift with an increase of sulfur fractions in the NCs, which can be ascribed to the size increases of CdS NCs. The maximum PL emission peak position of beads and string shows a red shift of about 100 and 50 nm as the S/Cd molar ratio increased from 0.03/1 to 0.12/1, respectively. We also have found that the PL intensity of NCs is also strongly influenced by the sulfur concentrations, in which the PL intensity first increases and then decreases with an increase of sulfur source molar fractions and achieves a maximum value at 0.06/1 (Figure 4b). Additionally, cupric ions doped CdS ($Cu_xCd_{1-x}S$) NCs loaded fluorescent hybrid microfibers using this single NC reaction were fabricated (Figure 4c). Taking advantage of the efficient mass transfer of microreactor, we observed the effect of cupric concentrations on the fluorescence intensity of microfibers. It is obviously seen from Figure 4d that the positions of peaks have a gradual red shift with an increase of the Cu^{2+} molar fraction, which can be attributed to the quantum confinement effect of an electron-hole pair, and the PL intensity of NCs decreases gradually. These experiments suggest that the microfluidic spinning system provides a novel and effective microreactor platform for in situ achieving high-performance fluorescent NCs and greatly facilitates for the controllable synthesis of fluorescent hybrid microfibers.

2.3. Production of Double-Metal Nanocrystals in Janus Microfiber Reactor

By designing microdevice with three-channel, dual reactions ($A+B_1 \rightarrow C_1$, $A+B_2 \rightarrow C_2$) were allowed to be simultaneously carried out in microfiber reactor and heterotypic Janus microfibers were obtained (Scheme 1b). **Figure 5**a displays the schematic diagram of coaxial flow microchannels in this three-channel microfluidic platform and illustrates the principles underlying the cross-linking and reaction process for the generation of

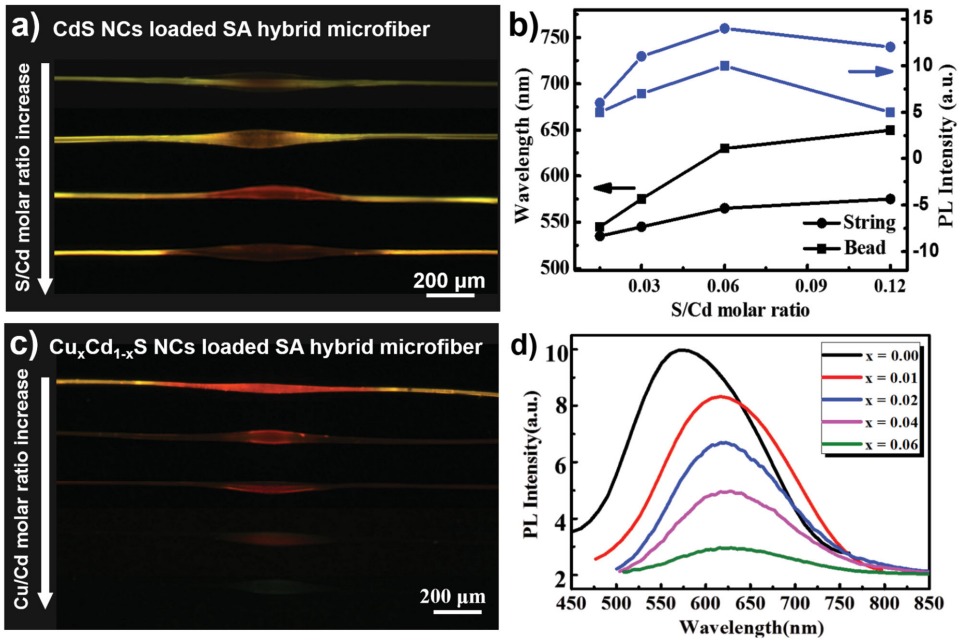

Figure 4. a) Fluorescent microscope images and b) the corresponding changes of PL intensity and emission peak position of string-of-beads CdA/CdS hybrid microfibers with different S/Cd molar ratio (0.015/1, 0.03/1, 0.06/1, and 0.12/1). c) Fluorescent microscope images of $Cu_xCd_{1-x}S$ NCs loaded alginate microfibers and d) the corresponding PL spectra.

Janus microfibers. In this case, 1 wt% SA/S^{2-} flow (A) was used as the sheath flow against two parallel needles containing 2 wt% Cd^{2+} solution (B_1) and 2 wt% $[Cu_{0.02}Cd_{0.98}]^{2+}$ solution (B_2) as core flows, respectively. In order to create Janus microfibers with symmetrical structure, it is crucially important to control the flow velocity of two miscible core phases. The optimal conditions for producing Janus microfiber in the system were controlled as follows: the flow rates of two core flows were

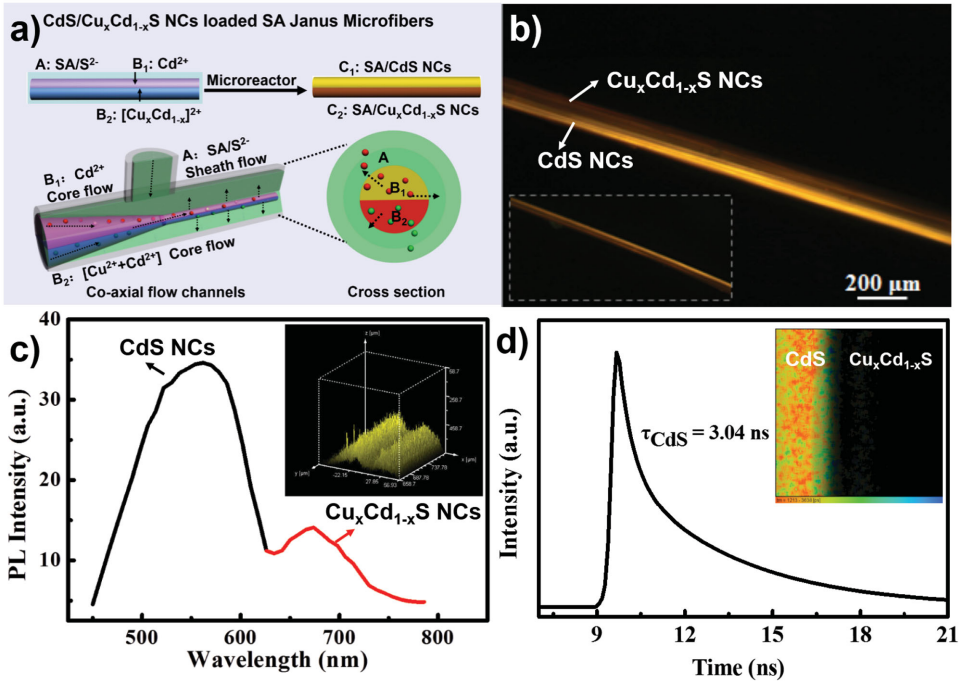

Figure 5. a) Schematic diagram of in situ synthesis of $CdS/Cu_{0.02}Cd_{0.98}S$ NCs loaded alginate Janus hybrid microfibers using the microfiber reactor. b) Fluorescent microscope images of CdS and $Cu_{0.02}Cd_{0.98}S$ NCs loaded alginate Janus hybrid microfibers. c) The corresponding PL emission spectra of CdS and $Cu_{0.02}Cd_{0.98}S$ NCs, inset: their corresponding PL intensity distribution of the patterns with a scaling factor of 0.4. d) The time-resolved fluorescence decay curves of the CdS NCs after one month, respectively. Insets: The corresponding fluorescence lifetime maps.

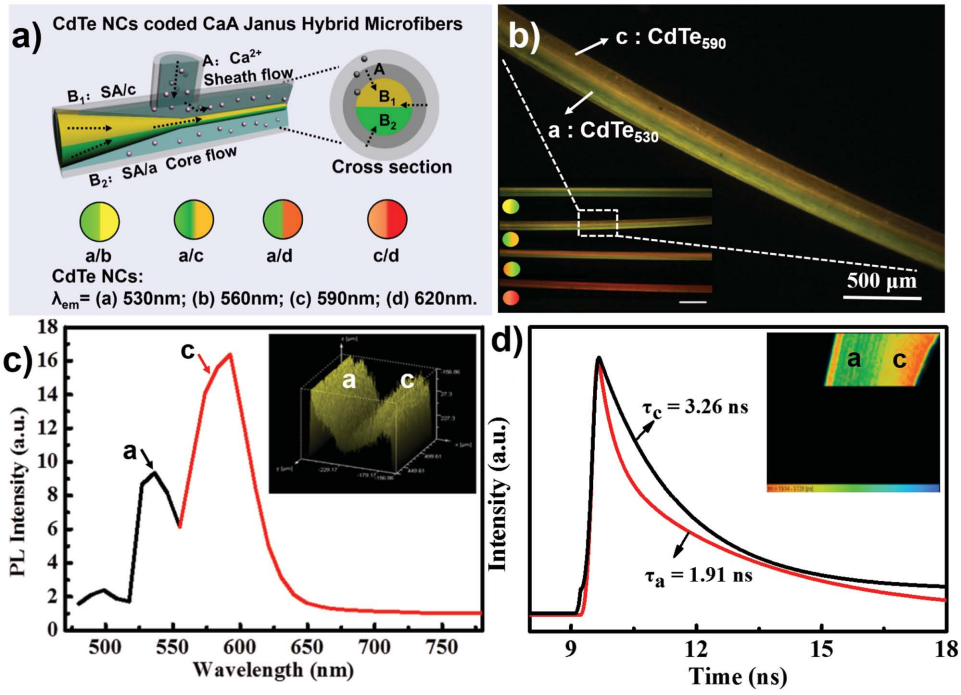

Figure 6. a) Schematic illustrations of the formation of CdTe NCs ($CdTe_{530}$, $CdTe_{560}$, $CdTe_{590}$, and $CdTe_{620}$) coded Janus alginate hybrid microfibers. b) Fluorescent microscope images of $CdTe_{530}/CdTe_{590}$ loaded alginate Janus hybrid microfibers. c) The corresponding PL emission spectra of CaA/CdTe Janus hybrid microfibers, inset: their corresponding PL intensity distribution of the patterns with a scaling factor of 0.4. d) The time-resolved fluorescence decay curves of the a/c after one month, respectively. Insets: The corresponding fluorescence lifetime maps.

similarly kept at 25 mL h^{-1}, and the sheath flow was fixed at 40 mL h^{-1}. The resulting $CdS/Cu_{0.02}Cd_{0.98}S$ NCs (C_1/C_2)-loaded Janus microfibers were synthesized with excellent fluorescent properties in a very short reaction time at room temperature. The utilization of dual reactions in microfiber reactor to facilely in situ fabricate different NCs loaded anisotropic microfibers has not been described previously. With this design, the microfiber reactor may open a new way to construction of compartmentalized microfibers with controllable fluorescent patterns, leading to a variety of applications, such as fluorescent codes, sensors, and optical devices. We expect that this design could endow the anisotropic hybrid fiber materials more flexibility and functionality.

In the following work, we have made efforts to encode different-sized CdTe NCs into CaA Janus microfibers via prescribed programs. As shown in **Figure 6**a, by varying the components of core flows, a series of CaA Janus fluorescent microfibers encoded with different particle sizes CdTe NCs, including a/b, a/c, a/d, and c/d (where a, b, c, and d represent differently sized CdTe NCs (λ_{em} = 530 nm (green), 560 nm (yellow), 590 nm (orange), and 620 nm (red), respectively,) were obtained. Figure S8 and Figure S9 (Supporting Information) show the fluorescent microscope images of encoded CaA/CdTe Janus microfibers and the corresponding PL spectra, which demonstrate the feasibility to fabricate versatile fluorescent hybrid materials using this platform. As the average Reynolds number of solutions in the microchannel was far from the transition point for turbulent flow, these fluids mainly formed laminar flows, so that no convective transport occurred across the adjacent streams. A clear and extremely sharp boundary can be seen at the interfaces of fibers doped with different compositions, as displayed in the optical images of prepared Janus microfiber (Figure 5b and Figure 6b), suggesting minimal mass transfer between these compartments. Furthermore, both the emission spectra and PL intensity distribution maps of $CdS/Cu_{0.02}Cd_{0.98}S$ NCs and $CdTe_{530}/CdTe_{590}$ NCs encoded Janus hybrid microfibers (Figure 5c and Figure 6c) show two components, corresponding to the specific optical properties of the NCs spatial separated in the Janus microfibers, which also indicate the formation of a well-aligned compartmentalized hybrid microfibers. The morphology of $CdTe_{530}/CdTe_{590}$ NCs encoded Janus microfibers by SEM (Figure S10, Supporting Information) further demonstrate that the surface structure of the fiber is uniform and there is no interface separation. To investigate the dynamical features of NCs loaded on Janus microfibers, we studied the temporal decay of the photoexcited state based on the TCSPC (Table S1, Supporting Information). Figure 5d and Figure 6d show the time-resolved fluorescence decay curves and corresponding fluorescence lifetime maps of $CdS/Cu_{0.02}Cd_{0.98}S$ NCs and $CdTe_{530}/CdTe_{590}$ loaded Janus microfiber after one month, respectively. Results demonstrate the simplicity, high efficiency, and flexible controllability of this microfluidic spinning system for the successful generation of NCs loaded anisotropic fluorescent microfibers, which might enable the fluorescent codes research and optical sensing applications. In addition, a variety of polymers chelated with ions are available, adding versatility to this inexpensive and easy-to-perform method.

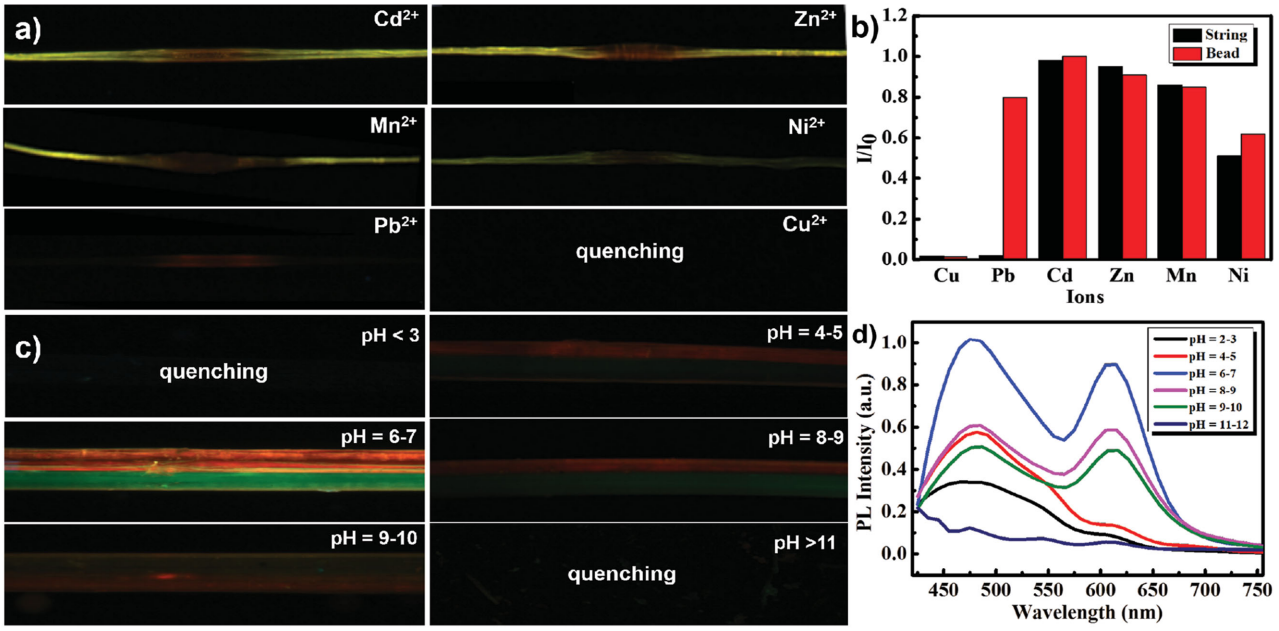

Figure 7. a) Fluorescent microscope images and b) the effects of metal ions on the relative PL intensity (I/I_0) of CdS NCs loaded string-of-beads CdA microfibers. The concentration of metal ions was fixed at 1×10^{-3} M. c) Fluorescent microscope images and d) PL emission spectra corresponding to the multiplexed analysis of different pH solutions by $CdTe_{530}/CdTe_{620}$ NCs loaded Janus hybrid microfibers.

2.4. Multiplexed Optical Analysis

It is well established that semiconductor NCs with unique photophysical properties have been developed into superior sensing material.[31,32] Various NC-based sensors were developed in the past few years, however, it is still rare that different-sized NCs are used as optical labels for multiplexed analytical assays.[33,34] For practical applications, we finally demonstrate the multiplexed analysis of metal ions and pH by using the different-sized NCs immobilized in the alginate hybrid microfibers. **Figure 7**a depicts the fluorescence response of CdS NCs loaded in string-of-beads CdA hydrogel microfibers to different metal ions. We can obviously see that the microfibers demonstrate PL completely quenching in the presence of Cu^{2+}, which could be attributed to the competitive carboxyl binding between the NC core and Cu^{2+}. The PL intensities of beads and string of the string-of-beads hybrid microfibers show different phenomena in the presence of Pb^{2+}: the PL of the string being completely quenched while the PL of bead decreased 20% (Figure 7b). This phenomenon is correlative with both the size and concentration of the CdS NCs. The selective response toward different metal ions suggests that the hybrid fluorescent microfibers could be suitable for optical probes. Similarly, exposing the Janus hybrid microfibers to different pH, NC-based sensors with two different optical signals were also observed. As shown in Figure 7d, both the PL intensities of $CdTe_{530}/CdTe_{620}$ NCs decrease with the increasing acidity and basicity of aqueous solution. This finding suggests that the microfiber reactors may constitute a new avenue to the fabrication of NC sensors for multiplexed optical sensing materials.

3. Conclusions

In summary, we proposed an easy-to-perform method to construct a robust fiber microreactor based on an MST as well as generate nanocrystals loaded anisotropic fluorescent hybrid microfibers. By programing coaxial flow microdevices with different geometric features, multiple nanocrystal reactions were carried out, and various anisotropic hybrid microfibers with string-of-beads and Janus microstructures and multiple fluorescent signals were fabricated for the first time. The advantage of this microfluidic spinning technology-directed microfiber reactors lies in its simplicity, high efficiency, flexible controllability, and environmental-friendly chemical process in the preparation of fluorescent nanocrystals and anisotropic hybrid microfibers. In addition, a variety of polymers jellified by ions could also be used as reaction substrates utilizing this method. We expect that this facile approach will lead to new anisotropic fluorescent hybrid materials with prospective applications in microreactors, multiplexed optical sensors, fluorescent codes, and neural-network-like biological materials.

4. Experimental Section

Materials: Sodium alginate (SA), sodium sulfide ($Na_2S{\cdot}9H_2O$), calcium dichloride ($CaCl_2$), chromium chloride ($CdCl_2{\cdot}2.5H_2O$), zinc chloride ($ZnCl_2$), and cupric chloride ($CuCl_2{\cdot}2H_2O$) were of analytical grade, commercially available and used without any further purification. Purified water with resistance greater than 18 MΩ cm^{-1} was used in all experiments. CdTe NCs were synthesized by our previously reported methods.[35]

Design of Microfluidic Spinning Equipment: The microfluidic spinning equipment has three major apartments that syringe

pumps (Model WZS-50F6, Smiths Medical Instrument Co., Ltd.) for stable velocity generation, coaxial flow-based microdevices with microchannels for microfiber generation and a roller for fiber receiver. Syringe pumps connected to the inlets were used to drive the sheath and core phase flows in the microchannels and a spinneret and bobbin system at the end of the output channel facilitated collection of the fibers for further examination.[23] The main functional units of this system are coaxial flow-based microdevices with microchannels for the generation of microfibers. The microdevice was made using a modified scaffold method developed by our previously reported work.[24]

Solid M-Alginate Microfibers: To prepare M-alginate microfibers, a half-T-shaped microfluidic device was fabricated by coaxially inserting a capillary tube with a 30 G needle (D = 0.51 μm) into a silicone rubber hose with inner diameter of 90 μm, which was fixed with ethyl α-cyanoacrylate instantaneous adhesive. The metal ions solution and the alginate solution were introduced into the rubber hose and the needle, respectively, at independently adjustable flow velocities using syringe pumps, and then transparent hydrogel fibers were formed at the outlet of microdevice.

String-of-Beads Microfibers: CdS NCs- and Cu-doped CdS ($Cu_xCd_{1-x}S$) NCs loaded alginate hydrogel microfiber with string-of-beads structures in the same way using this half-T-shaped microdevice were fabricated. Typically, for the in situ synthesis of CdS NCs loaded microfiber (S/Cd molar ration: 0.03/1), $CdCl_2{\cdot}2.5H_2O$ (0.3426 g, 1.5 mmol) were simultaneously dissolved in 20 mL of deionized water, used as the sheath flow phase. Subsequently, 1 mL $Na_2S{\cdot}9H_2O$ (0.045 M) aqueous solution was added into 20 mL SA phase (1 wt%) and mixed with stirring, used as core flow. The fluorescent microfibers with string-of-beads were obtained after solvent evaporation at room temperature. For the synthesis of $Cu_{0.02}Cd_{0.98}S$ NCs (x = 0.02), $CdCl_2{\cdot}2.5H_2O$ (0.3357 g, 1.47 mmol) and $CuCl_2{\cdot}2H_2O$ (0.0071 g, 0.03 mmol) simultaneously dissolved in 20 mL of deionized water was used as the gelation phase. By changing the value of x, namely, x = 0.00, 0.01, 0.04, and 0.06, $Cu_xCd_{1-x}S$ NCs with different compositions can be obtained, keeping the total molar weight of $[Cd^{2+} + Cu^{2+}]$ = 1.5 mmol.

Janus Microfibers: For the fabrication of Janus microfibers, our basic microfluidic device underwent a transformation, paired capillaries were used instead of the single needle to force two different core flow to flow simultaneously. Typically, for the synthesis of $CdS/Cu_{0.02}Cd_{0.98}S$ NCs loaded Janus microfiber, one of the core flowing liquids was the $CdCl_2$ solutions (2 wt%) and the other was the $[Cu_xCd_{1-x}]Cl_2$ solutions (2 wt%). For the synthesis of $CdTe_{530}/CdTe_{590}$ NCs loaded Janus CaA hybrid microfibers, one of the core flowing liquids was the alginate solution (1 wt%) mixed with $CdTe_{530}$ NCs and the other was the alginate solution (1 wt%) mixed with $CdTe_{590}$ NCs.

Measurements: Photographs and observations of microstructures of fluorescent microfibers were obtained using a Zeiss AXIO 5 Imager optical microscope. Photoluminescence (PL) spectra and microscopic views of the fluorescent microfibers were achieved on a laser scanning confocal microscope (LSCM). The optical images were taken using an Olympus MVX10 stereomicroscope with color CCD camera. IR images were performed on a Thermo Scientific Nicolet iN10 infrared microscope equipped with a liquid nitrogen cooled MCT detector (Thermo Electron Corporation, USA). IR microscopy data were collected using reflection mode. IR spectra were captured using an aperture size of 50 μm by 50 μm and were recorded over a range of 650–4000 cm^{-1}. XRD pattern was conducted on a Bruker-AXS D8 ADVANCE X-ray diffractometer with CuKα radiation (λ = 0.1542 nm) at a scanning speed of 60 rpm over a 2θ range of 10°–80°. Transmission electron microscopy (TEM) observation was performed with a JEOL JEM-2010 TEM. The morphology of the microfluidic spinning fibers was observed by scanning electron microscopy (SEM) with a QUANTA 200 (Philips-FEI, Holland) instrument at 20.0 kV. Time-resolved fluorescence decay curves were achieved on an Edinburgh FL 900 photocounting system. The thermogravimetric analyses (TGA) were obtained with a NETZSCH STA 409 PC in N_2 flow in the temperature range 40–700 °C, the heating rate being 10 °C min^{-1}.

Supporting Information

Supporting Information is available from the Wiley Online Library or from the author.

Acknowledgements

This work was supported by National Natural Science Foundation of China (21076103, 21474052, and 21176122), Priority Academic Program Development of Jiangsu Higher Education Institutions (PAPD), and Qing Lan Project.

Received: August 31, 2015
Published online: November 5, 2015

[1] J. H. Jung, C. H. Choi, S. Chung, Y. M. Chung, C. S. Lee, *Lab Chip* **2009**, *9*, 2596.
[2] D. M. Lavin, R. M. Stefani, L. Zhang, S. Furtado, R. A. Hopkins, E. Mathiowitz, *Acta Biomater.* **2012**, *8*, 1891.
[3] C. Meng, Y. Xiao, P. Wang, L. Zhang, Y. Liu, L. Tong, *Adv. Mater.* **2011**, *23*, 3770.
[4] H. Onoe, T. Okitsu, A. Itou, M. Kato-Negishi, R. Gojo, D. Kiriya, K. Sato, S. Miura, S. Iwanaga, K. Kuribayashi-Shigetomi, Y. T. Matsunaga, Y. Shimoyama, S. Takeuchi, *Nat. Mater.* **2013**, *12*, 584.
[5] S. J. Hurst, E. K. Payne, L. D. Qin, C. A. Mirkin, *Angew. Chem. Int. Ed.* **2006**, *45*, 2672.
[6] K. J. Lee, T. H. Park, S. Hwang, J. Yoon, J. Lahann, *Langmuir* **2013**, *29*, 6181.
[7] X. L. Tian, H. Bai, Y. M. Zheng, L. Jiang, *Adv. Funct. Mater.* **2011**, *21*, 1398.
[8] S. Bhaskar, J. Lahann, *J. Am. Chem. Soc.* **2009**, *131*, 6650.
[9] Y. Cheng, F. Zheng, J. Lu, L. Shang, Z. Xie, Y. Zhao, Y. Chen, Z. Gu, *Adv. Mater.* **2014**, *26*, 5184.
[10] Y. Jun, E. Kang, S. Chae, S. H. Lee, *Lab Chip* **2014**, *14*, 2145.
[11] C. H. Choi, H. Yi, S. Hwang, D. A. Weitz, C. S. Lee, *Lab Chip* **2011**, *11*, 1477.
[12] E. Kang, G. S. Jeong, Y. Y. Choi, K. H. Lee, A. Khademhosseini, S. H. Lee, *Nat. Mater.* **2011**, *10*, 877.
[13] M. Yamada, S. Sugaya, Y. Naganuma, M. Seki, *Soft Matter* **2012**, *8*, 3122.
[14] Y. Yu, H. Wen, J. Ma, S. Lykkemark, H. Xu, J. Qin, *Adv. Mater.* **2014**, *26*, 2494.
[15] X. H. Ji, W. Cheng, F. Guo, W. Liu, S. S. Guo, Z. K. He, X. Z. Zhao, *Lab Chip* **2011**, *11*, 2561.
[16] G. R. Bardajee, Z. Hooshyar, *Spectrochim. Acta A* **2013**, *114*, 622.
[17] K. S. Elvira, X. C. i Solvas, R. C. R. Wootton, A. J. deMello, *Nat. Chem.* **2013**, *5*, 905.
[18] J. L. Steinbacher, D. T. McQuade, *J. Polym. Sci., Part A: Polym. Chem.* **2006**, *44*, 6505.
[19] T. W. Phillips, I. G. Lignos, R. M. Maceiczyk, A. J. deMello, J. C. deMello, *Lab Chip* **2014**, *14*, 3172.
[20] L. Zhang, Y. Xia, *Adv. Mater.* **2014**, *26*, 2600.
[21] I. Lignos, L. Protesescu, S. Stavrakis, L. Piveteau, M. J. Speirs, M. A. Loi, M. V. Kovalenko, A. J. deMello, *Chem. Mater.* **2014**, *26*, 2975.
[22] A. M. Nightingale, J. C. deMello, *Adv. Mater.* **2013**, *25*, 1813.
[23] L. L. Xu, C. F. Wang, S. Chen, *Angew. Chem. Int. Ed.* **2014**, *53*, 3988.
[24] S. N. Yin, C. F. Wang, Z. Y. Yu, J. Wang, S. S. Liu, S. Chen, *Adv. Mater.* **2011**, *23*, 2915.
[25] C. G. van Hoogmoed, H. J. Busscher, P. de Vos, *J. Biomed. Mater. Res. A* **2013**, *67A*, 172.
[26] M. K. Mallappa, R. Kesarla, S. Banakar, *J. Drug Delivery* **2015**, *2015*, 826981.

[27] I. Yoo, S. Song, B. Yoon, J. M. Kim, *Macromol. Rapid Commun.* **2012**, *33*, 1256.
[28] J. Owen, *Science* **2015**, *347*, 615.
[29] Y. P. Hou, L. C. Gao, S. L. Feng, Y. Chen, Y. Xue, L. Jiang, Y. M. Zheng, *Chem. Commun.* **2013**, *49*, 5253.
[30] L. R. Hou, L. Chen, S. Chen, *Langmuir* **2009**, *25*, 2869.
[31] R. Freeman, T. Finder, I. Willner, *Angew. Chem.* **2009**, *121*, 7958.
[32] J. S. Han, X. Zhang, Y. B. Zhou, Y. Ning, J. Wu, S. Liang, H. C. Sun, H. Zhang, B. Yang, *J. Mater. Chem.* **2012**, *22*, 2679.
[33] X. H. Ji, W. Cheng, F. Guo, W. Liu, S. S. Guo, Z. K. He, X. Z. Zhao, *Lab Chip* **2011**, *11*, 2561.
[34] A. W. Zhu, Q. Qu, X. L. Shao, B. Kong, Y. Tian, *Angew. Chem.* **2012**, *124*, 7297.
[35] X. Guo, C. F. Wang, Y. Fang, L. Chen, S. Chen, *J. Mater. Chem.* **2011**, *21*, 1124.